J. Coat. Technol. Res., **20** (6) 1997–2006, 2023
https://doi.org/10.1007/s11998-023-00793-4

Low-cost fabrication and physicochemical characterization of $ZnFe_2O_4$ nanoparticles as an efficient multifunctional inorganic pigment

Mostafa A. Sayed, W. M. A. Abdelmaksoud, Said M. Teleb, Adel M. El-Din, Mohamed M. Abo-Aly

Received: 28 August 2022 / Revised: 31 March 2023 / Accepted: 11 April 2023

Abstract The pursuit of low-cost manufacturing of newly effective pigments is a pressing economic need. Thus, in this work, low-cost $ZnFe_2O_4$ spinel nanoparticles (ZF-NPs) with an average diameter of 20 nm were successfully synthesized using a simple sol–gel method, which can be extended for large-scale fabrication of a reddish nano pigment. TGA/DTA, XRD, DRS, HRTEM, and SEM/EDX investigations were used to characterize the as-prepared product. The color of synthesized NPs was studied using CIE $L^*a^*b^*$ colorimetric method with color coordinates of $L^* = 41.7$, $a^* = 72.2$, and $b^* = 48.8$. The newly developed pigment was examined to be superior to the traditional pigment (M6001/Fe_2O_3: $L^* = 30.4$, $a^* = 42.16$, and $b^* = 45.7$). After that, the synthesized nano pigment was integrated into both ink and paint formulations as a multifunctional coating. The inclusion of synthesized nano pigment in metal coating printing ink formulation was done to produce a good alternative and cost-effective substitute for the commercially available pigment used in the inks industry. Also, the effect of the fabricated nanoparticles on corrosion resistance and thermal stability of epoxy-based paint formulations was evaluated using different standard tests. Therefore, the $ZnFe_2O_4$ pigment should be applied as a highly efficient inorganic nano pigment.

M. A. Sayed (✉), M. M. Abo-Aly
Chemistry Department, Faculty of Science, Ain Shams University, Cairo, Egypt
e-mail: mostafa_abdellah@sci.asu.edu.eg

W. M. A. Abdelmaksoud, A. M. El-Din
Paint and Chemicals Industries (Pachin) Co., Cairo, Egypt

S. M. Teleb
Chemistry Department, Faculty of Science, Zagazig University, Zagazig, Egypt

Keywords Zinc ferrites, Inorganic pigments, Anticorrosive properties, Spectroscopic analysis, Physicochemical characteristics

Introduction

The coatings industry has recently shown a great deal of interest in the use of nanoparticles because of the ways in which they improve paints and bring about new features.[1] Nanoparticle use in coatings has been shown to improve coating performance as well as add new functions to the system, enabling the development of coatings with multiple uses. Resistance to abrasion, erosion, and chemicals, UV light resistance, antifouling qualities, and other advantages of nanomodified paint are just few examples.[2]

Coatings are indispensable to our daily lives. Coated materials today cover a wide range of products we use in our daily lives, including our homes and other materials for a variety of reasons, including decorative, protective, and utilitarian, but in most cases, a combination of these considerations is used.[3] The term ''multi-functional coatings'' refers to a single-layered coat that can perform multiple functions. These coatings could provide decoration and protection, as well as additional features such as self-cleaning, easy-to-clean, anticorrosion, thermal stability, and antibacterial properties, among others. Preparing multifunctional coatings could also assist to reduce costs, as well as overcome the drawback of a multilayered system, in which the activities are separated. In a multilayered system, coating activities are influenced by each layer in the system, and if one layer is distorted, the entire system is disrupted.[4,5]

Nowadays, inorganic pigments have been used in many fields in industry such as plastic, polymer, paints, ink, glasses, and ceramics. Most of these pigments are metal-based compounds.[6] Pigments with particle size

in the nanoscale are more important in the market since they have higher surface area, which translates to a better surface coverage, a higher number of reflectance points and therefore improved color scattering.[7,8]

For many years, ferrite pigments containing spinel structures have been researched. Typically, they produce high-quality, heat-stable, tan-colored pigments with great thermal stability that are suited for a variety of demanding purposes.[9–11] The extremely significant class of inorganic pigments known as anticorrosive pigments are characterized by an inhibitory effect when added to paintings.[12] Spinel pigments are representative of the large category of potential anticorrosive pigments.[13] The spinel structure, denoted by the formula AB_2O_4, is comprised of a virtually cubic arrangement of oxygen, with the cations occupying tetrahedral and octahedral interstitial sites.[14,15] The spinel pigments are extremely durable and maintain their color in a lot of circumstances. The activity of the common ferrite pigments is predicated on their hydrolysis in the coating. In this process, hydroxides are created, which act as a corrosion inhibitor and counteract the creation of soaps of alkaline earth metals in some binders (alkyds, epoxy esters), passivation caused by the presence of OH– ions, and corrosion brought on by the higher pH.[10,16]

Most nano inorganic pigments, which are blends of metal oxides, are created utilizing a variety of techniques. Quite frequently, the preparation would begin with the mixing of oxides, calcination at high-temperatures, typically higher than 1200 °C, and then crushing to guarantee correct particle size distribution of powders.[17] Sol–gel, emulsion precipitation, hydrothermal method, low combustion approach, and others are also employed to create inorganic pigment.[18–21] Simple procedures like sol–gel and solid state chemical reactions produce mixed oxides with large specific surface area and uniform particle sizes.[22–24] Recently, various mixed metal oxides that are nanosized were created as novel high heat- and/or corrosion-resistant pigments, including Ca_2CuO_3, $Ca_3Co_2O_6$, and $NiSb_2O_6$.[25,26] Color, particle size, and durability in acidic and alkaline conditions are just some of the physicochemical aspects of inorganic pigments that can be significantly impacted by the synthesis process chosen.[5,27,28]

Lately, non-toxic anticorrosive pigments based on iron oxide and oxides of divalent metals in ferrites of various colors have been created; these ferrite pigments exhibit improved corrosion protection.[29,30] They are increasingly frequently employed in coating and plastic compositions that require both low toxicity and great processing stability due to their increasing popularity.[31] We discovered by looking through the literature that additional study is still required to develop more efficient nanosized pigments for the coatings industry. Consequently, in the current study, a multifunctional coating based on low-cost zinc ferrite nanoparticles (ZF-NPs) with high chromaticity (a^*) was created using the favorable sol–gel process. The solid pigments were identified through TGA/DTA, XRD, HRTEM, SEM/EDX, DRS analyses. The synthesized reddish pigment was also applied in printing inks formulation and as an anticorrosive pigment.

Experimental

Materials

To reduce the economic cost, the chemicals and solvents utilized in this study to produce nanoparticles were obtained commercially and employed without additional purification. Zinc acetate hydrate ($Zn(CH_3COO)_2{\cdot}2H_2O$), ferric chloride hydrate ($FeCl_3{\cdot}6H_2O$), cetyl-trimethyl-ammonium-bromide (CTAB), ammonium hydroxide (NH_4OH, 28%), and absolute ethanol (C_2H_5OH) were supplied from Adwic company, Egypt.

Synthesis of $ZnFe_2O_4$ NPs

The efficient sol–gel technique was used to fabricate spinel $ZnFe_2O_4$ nanoparticles (ZF-NPs) on a massive scale, as documented in the literature.[32] In a typical procedure, a solution containing 10.97 g of $Zn(Ac)_2{\cdot}2H_2O$ was combined with $FeCl_3{\cdot}6H_2O$ solution (27.03 g, 100 mL) in the presence of 2.0% (w/v) CTAB to retain a molar ratio molar ratio of (1 Zn^{2+}:2 Fe^{3+}). The mixture was violently swirled for 1 h at room temperature, then NH_4OH (28%) was drop wisely added to the mixture with regular stirring until the desired pH was reached (9–10). The suspension was aged for 24 h after complete precipitation. The resulting reddish-brown residue was refined, rinsed multiple times with deionized water, and dried at 80 °C overnight, yielding spinel dry hydrogel. TGA/DTG thermogram of the spinel dried gel is shown in Fig. 1. Finally, after drying, the sample was ground and calcined in an air muffle at a temperature of 500 °C for 3 h. ZF-NPs were the

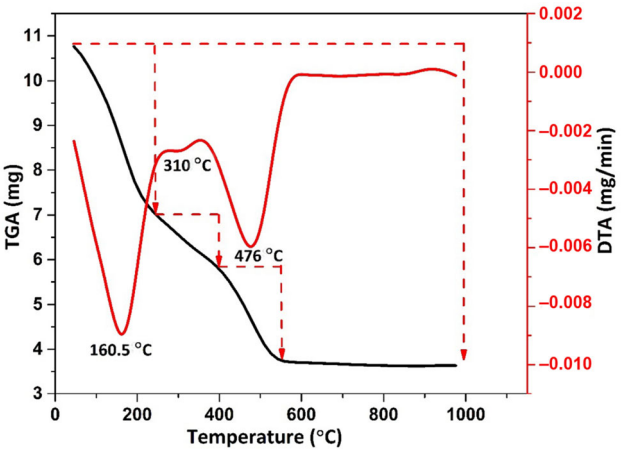

Fig. 1: TGA/DTA curves of as-synthesized dried gel

designation given to the blasted sample for further experimental work.

Instrumentation

Thermal gravimetric analyzer (TGA/DTG, PerkinElmer, USA) and X-ray diffraction (XRD, RigakuD/MAX 2550, k140.15418 nm) were used for phase configuration identification. Scanning electron microscopy (SEM/EDX, JEOLJSM-7500F) was also used to examine the surface morphology of the synthesized specimens. Characterizations were carried out using a JEOLTEM-2100 apparatus for (HRTEM) studies. On a Shimadzu UV-2700 spectrophotometer, UV–visible spectra in the 200–800 nm range were obtained.

Pigment evaluation

Physicochemical measurements

Color test (ASTM D387), melting point test (ASTM D127), oil absorption test (ASTM D281) and specific gravity test (ASTM C329) were carried out at Pachin Company according to standard methods.[33–35] The ''Commission Internationale de l'Eclairage (CIE)'' used and recommended the CIE 1976 $L^*a^*b^*$ colorimetric method in the range of 200–800 nm using ten standard observed angles, D65 illumination, and a white standard.[36] Three parameters (L^*, a^*, and b^*) are used as color axes in this method. The first two are called a^* and b^* hue dimensions. The blue color is linked to the negative value of b^*. The positive value has to do with yellow color. The green color is linked to the negative value of a^*. Red is a positive color and has a positive value. The third is L^*, which stands for lightness axis that has a value of 0 for black and a value of 100 for white and CIElab difference ΔE, is calculated by $\Delta E = \sqrt{[(L^*)^2 + (a^*)^2 + (b^*)^2]}$.

Diffuse reflectance UV–Vis spectroscopy (DRS) analysis

All the synthesized samples' optical absorbance spectra are measured between the wavelengths of 200 and 800 nm. The samples' bandgap energies are then inferred from those spectra. The direct bandgap energy (E_g) of as-synthesized samples was determined by fitting the absorption data to the direct transition equation (Tauc's equation):[37]

$$(\alpha h\upsilon)^2 = A\left(h\upsilon - E_g\right) \quad (1)$$

where α is the absorption coefficient, $h\upsilon$ is the photon energy, E_g is the direct bandgap of the material and A is constant.

The bandgap energies of as-prepared samples have been measured by plotting $(\alpha h\upsilon)^2$ as a function of photon energy ($h\upsilon$) and extrapolating the linear portion of the curve to an absorption equal to zero.[21,38]

Corrosion tests

Accelerated corrosion laboratory test

A 1 mm X scribe was carved on the dry coated film to expose the underlying steel to the aggressive medium for 28 days. Following the exposure period, the panels were evaluated for the following characteristics: degree of rusting under film (ASTM D 610-00), degree of blistering on coated steel panel according to (ASTM D 714-07), degree of coating adhesion by a cross-cut test (ASTM D 3359-97), and filiform corrosion resistance test was conducted by photographic detection according to (ASTM D 2803-93).

Electrochemical impedance spectroscopy (EIS)

In a three-electrode cell configuration, SCE, platinum spiral and panel covered with coatings were used as reference counter and working electrodes. EIS measurements were done in the frequency range of 10 and 20 mHz and by applying 20 mV sinusoidal perturbation in accordance with the principles of EIS investigation of high resistance coating. The impedance spectra for different Nyquist plots were analyzed by fitting the experimental data to a simple Randles circuit mode [$R_s + C_{dl}/R_{ct}$)] as shown in Fig. 2. The equivalent circuit represents the corrosion process on the bare surface, and it consists of the electrolyte resistance (R_s) in series with both double layer capacitance (C_{dl}) and charge-transfer resistance (R_{ct}) which are in parallel with each other.

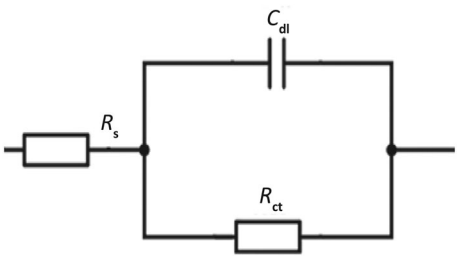

Fig. 2: Equivalent electrical circuit used to fit the EIS data of the coated film

Results and discussion

Characterization of the fabricated ZF-NPs

Powder XRD (X-ray diffraction) analysis was done to confirm the crystallinity and phase purity of the newly made nano pigment. The powder XRD patterns of synthesized $ZnFe_2O_4$ NPs (Fig. 3) shows diffraction peaks indexed at (111), (220), (311), (222), (400), (331), (422), (511), (440), (531), (620), (533), and (444) planes. Similar XRD pattern for nanosized $ZnFe_2O_4$ has also been observed by several reports.[39,40] The XRD pattern revealed no extra peaks, confirming the purity of the sample. As a result, the diffraction patterns obtained indicated the creation of pure, crystalline, and single-phase materials with Fd-3m space group cubic spinel zinc ferrite nanostructure (JCPDS 82-1049).[41] The mean crystallite size of the manufactured sample is estimated from the full-width-half-maximum (FWHM) of the fundamental diffraction peaks utilizing the Scherrer equation:[20]

$$D = \frac{k\lambda}{\beta \cos\theta} \tag{2}$$

where D is the crystallite size, λ is the wavelength of the incident X-ray radiation, typically 1.54 Å, θ is the Bragg angle, β is the FWHM in radians and k is the shape factor equal to 0.89. The average crystallite size of synthesized $ZnFe_2O_4$ NPs was found to be 22.5 nm.

Figure 4 shows TEM image of ZF sample generated through dispersion in alcohol. It was discovered that the particles are virtually spherical and within nanoscale size of 20 nm. The results also reveal a narrow particle-size fluctuation throughout the micrograph's field. In addition, the surface morphology of the produced pigment in concern was examined using a scanning electron microscope (SEM) at a tenfold magnification, as shown in Fig. 5a. The crystals ranged in size from nanometer (about 30 nm) to micrometers (approximately 10 μm) and gave homogenous particle size. Energy dispersive X-ray spectroscopy (EDX) was

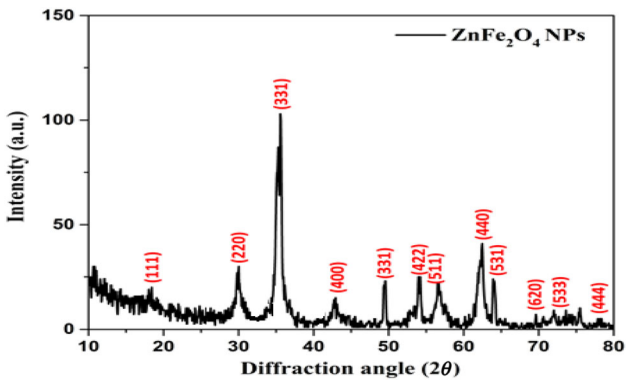

Fig. 3: Powder X-ray diffractograph of $ZnFe_2O_4$ nanostructure

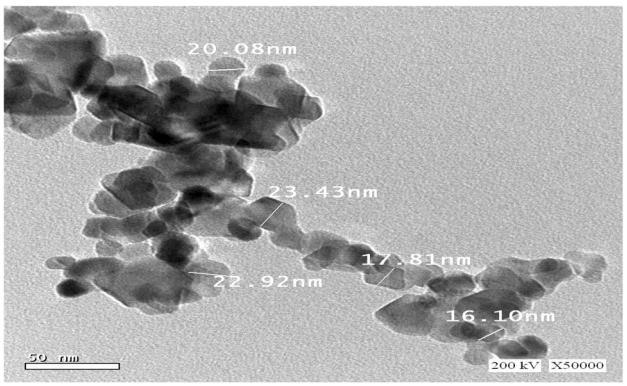

Fig. 4: TEM micrograph of synthesized ZF pigment by sol–gel approach

also used to investigate the purity and elemental composition of $ZnFe_2O_4$ nanostructure as illustrated in Fig. 5b. It is abundantly evident that the manufactured $ZnFe_2O_4$ nanostructure did not include any form of elemental contaminants with purity of 100%. As a result, this approach can be used to make nanoparticulated pigment in industry.

The solid state DRS of the synthesized nano pigment are displayed in Fig. 6. ZF nanostructure shows a sharpening at 350 nm and light absorption tails at about 700 nm, supporting that the as-prepared material has a wide visible light absorption range.[42] For materials with narrow bandgaps, the optical absorption coefficient of zinc ferrite is consistent with Tauc's equation.[43,44] The bandgap value derived from the absorption spectra of ZF sample was found to be 1.7 eV. It is reported also that the estimated bandgaps of the iron oxide red, M6001/ZF-NPs, and M6001/iron oxide red pigments are 2.2, 1.75, and 2.22 eV, respectively. Accordingly, the red color coordinate a^* being 72.22 vs 42.16 of the commercial pigment (M6001/Fe_2O_3), is significantly higher (Table 1) indicating the higher potential of the synthesized ZF-NPs as basis for new efficient red pigments. The correlation between bandgap energies and the coloristic appearance of materials becomes apparent in this study as reported in recent work.[45] Smaller bandgaps allow light with lower energy to excite electrons from the valence into the conduction band, which causes the absorption of the respective wavelength ranges. Therefore, the colors of the materials change because of reflection at various wavelengths. In our situation, the pigments absorb more yellow light (red shift) as a result of the smaller bandgap, giving rise to a more striking reddish appearance.[45,46]

Applications of the synthesized ZF nano pigment

Printing ink industry

The new nano inorganic pigment $ZnFe_2O_4$ NPs was formulated with metal coating ink as epoxy resin

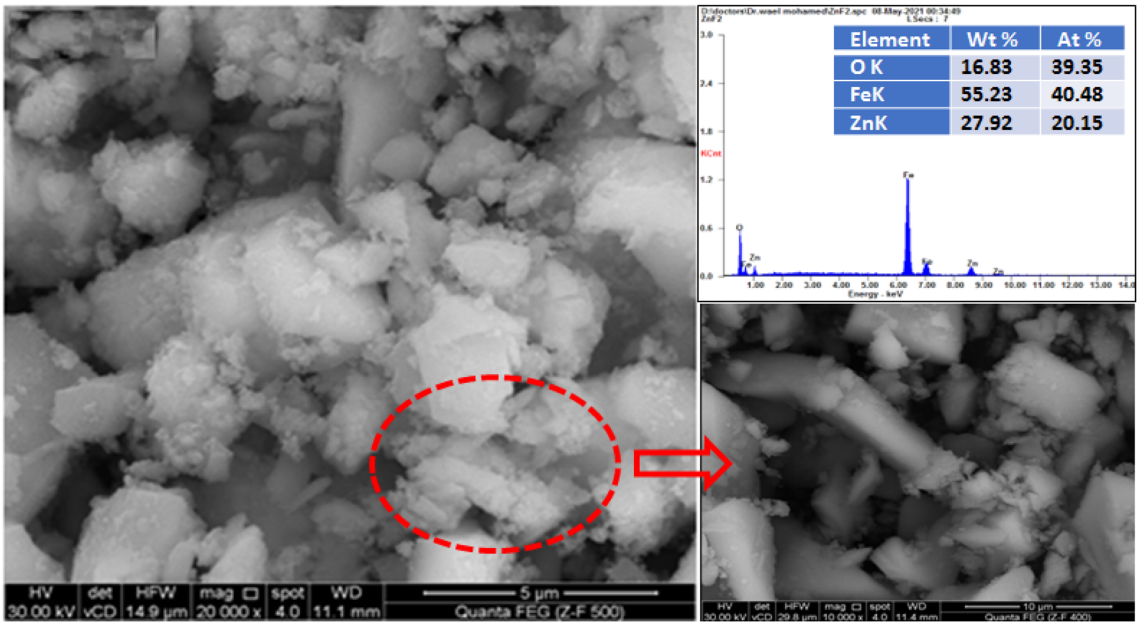

Fig. 5: SEM/EDX images of $ZnFe_2O_4$ spinel nanoparticles

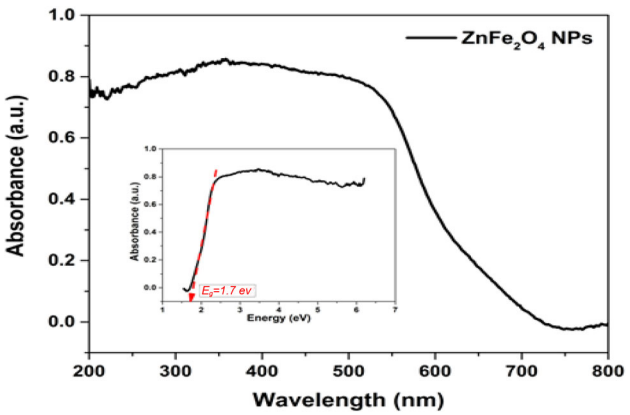

Fig. 6: Solid state UV–Vis spectra of synthesized ZF nano pigment

Table 1: CIE *L*a*b color coordinates of synthesized ZF and M6001 pigments**

Sample	*L**	*a**	*b**	E_g/ eV	ΔE
ZF-NPs	41.72	72.22	48.80	1.7	1.07
Iron Oxide Red	41.48	72.60	49.76	2.2	
M6001/ZF-NPs	30.86	41.81	45.32	1.75	0.68
M6001/Iron Oxide Red	30.45	42.16	45.72	2.22	

binder and butyl glycol as solvent as shown in Table 2. These new printing inks have been applied on metals or tin substrate at room temperature (25 °C). Their efficiency was compared to the commercial printing inks which already exist in Pachin Company (Egypt). Figure 7 shows the color appearance clarity of the new printing inks containing the new nano inorganic pigments $ZnFe_2O_4$ NPs compared to M6001. The visual inspection of the printing ink containing new nano inorganic pigments $ZnFe_2O_4$ NPs showed that its color was typically similar to the color of the commercial ink (M6001) with lower pigment loading of 40% versus 60%. The prepared inks were stable at the room temperature without any change or decomposition. Furthermore, after 6 months of storage, the produced ink samples showed no change in color or viscosity or when used in printing as mentioned in Fig. 8. These results are very promising and prove that the prepared nano pigment has high efficiency with low economic cost in this application. Therefore, the creation of this new nanosized pigment can be used locally as an alternative to traditional imported pigments.

Anticorrosive paint performance

The new inorganic pigment ZF-NPs was formulated in paints industry as epoxy resin, a binder, and xylene as solvent as shown in Table 3. The corrosion resistance of the produced nano pigment is evaluated here.

Accelerated corrosion laboratory test

Table 4 summarizes the results of a 28-day immersion test in sea water (3.5 percent NaCl) for a paint film incorporated with ZF-NPs. According to the results, the coat incorporating ZF nano pigment has a high

Table 2: Metal coating ink formulations according to Pachin company

Raw material	M6001	
	Standard	Sample (nano pigment)
Epoxy resin	24.4	26.4
Solvent naphtha 100	12.81	12.81
Butyl glycol	23.79	23.79
Disper-BYK-163	1	1
$ZnFe_2O_4$ NPs	0	4
Iron oxide red	6	0
Butylated benzoguanamine resin	10	10
n-Butyl acetate	10	10
Butyl glycol	5	5
Phosphoric acid	0.1	0.1
Silicon slip additive	0.5	0.5
Solvent naphtha 100	4	4
Solvent naphtha 100	2.4	2.4
Total	100	100

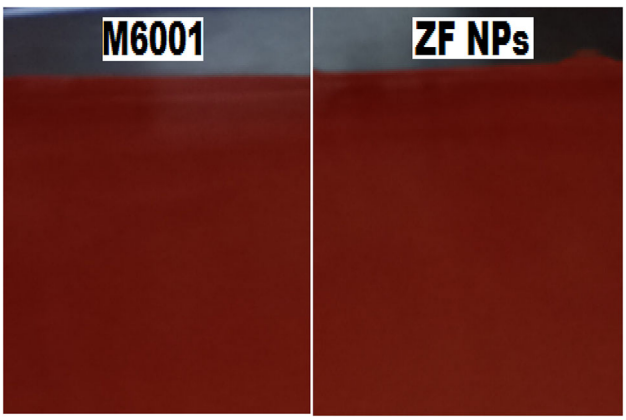

Fig. 7: The visual inspection of the prepared printing inks containing (M6001 and new nano inorganic pigment ZF-NPs)

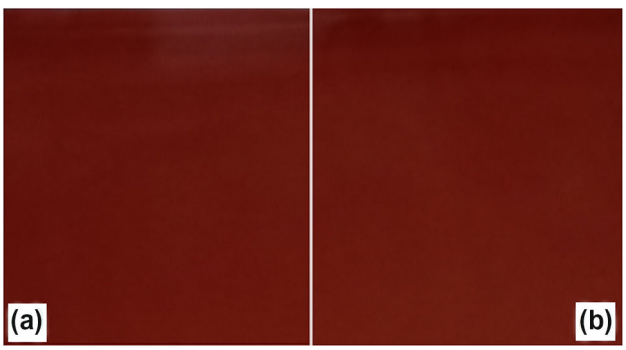

Fig. 8: The visual inspection of the prepared printing inks containing $ZnFe_2O_4$ nano pigment (a) before (b) after six months of storage

Table 3: Paint formulation incorporating ZF nano pigment

Ingredients (gm)	Sample (nano pigment)
Epoxy resin	32
Fe_2O_3	18
TiO_2	7
Kaolin	18
$BaSO_4$	5
$ZnFe_2O_4$	20
Total pigment	68
Total	100
Pigment/binder ratio	2.125

level of adhesion, as shown in Fig. 9. The presence of aliphatic hydroxyl and ether groups in the epoxy resin chain and the cured epoxy polymer may contribute to the high polarity of the epoxy resin chain and the cured epoxy polymer.[47] The presence of ZF-NPs on the treated steel surface creates a powerful electromagnetic attraction between the two materials. The hydroxyl group concentration of the epoxy compound is directly proportional to the coating adhesion strength to steel. Coating adhesion is increased by the formation of chemical interactions between active hydrogen on the steel surface and epoxide groups in the coating.[48] The lack of blisters on the coat was due to the good adhesion. Moreover, the coated film containing nano zinc ferrite pigment has a promising corrosion resistance.

Table 4: Corrosion results of the coated film after immersion in 3.5% NaCl for 28 days

Test	Nano pigment	Description
Degree of blistering	10	There are no blisters formed on the film
Rust under film	10	There is no rust under film after elimination of the coat
Adhesion	Gt1	Adhesion can be ordered in descending order as follows; Gt0 > Gt1 > Gt2 > Gt3 > Gt4, thus adhesion of the coat is very good

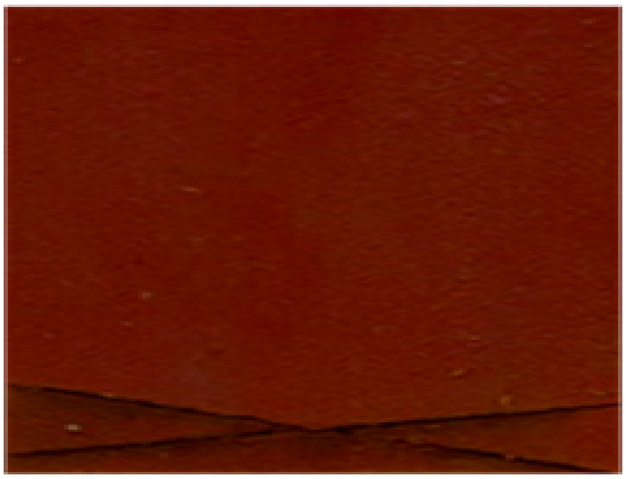

Fig. 9: Immersion test results ZF-NPs-coated film after immersion in 3.5% NaCl for 28 days

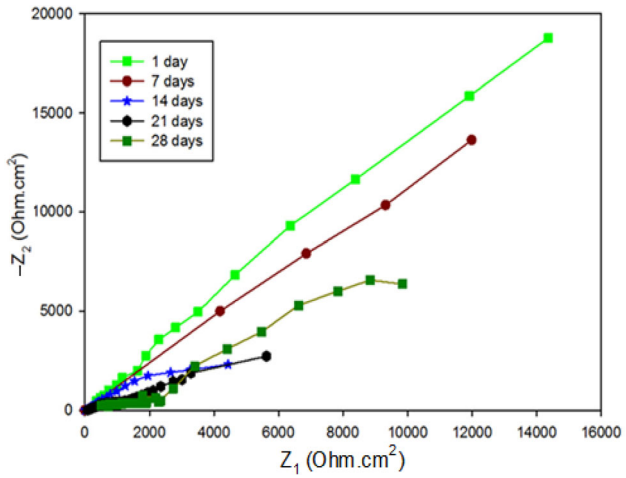

Fig. 10: Nyquist plot of the ZF-NPs-coated film after 3.5% NaCl for 28 days

Table 5: EIS data of the ZF-NPs-coated film

Sample	Days	R_{ct} (Ohm cm^2)
Nano pigment	1 day	11,769
	7 days	8305
	14 days	3200
	21 days	5651
	28 days	6439

Electrochemical impedance (EIS) results

Table 5 and Fig. 10 provide the impedance data and Nyquist plot of the coated film after 28 days of seawater immersion. The experimental results were compared to the corresponding simple Randles circuit is shown in Fig. 2. The charge-transfer resistance was 11,769 Ohm cm^2 on the first day, according to the impedance data in Table 5, and then gradually decreased until 14 days. The charge-transfer resistance increases again between 21 and 28 days due to the creation of a passive layer. The production of porous, soluble hydroxide precipitates over cathodic sites is linked to the anticorrosion action of ferrites in coatings.[49–51] Cathodic current is reduced by partially blocking the cathodic sites, which also lowers total corrosion. The production of porous, insoluble hydroxide precipitates over cathodic sites is related to ferrites' anticorrosion mechanism in coatings. By partially blocking the cathodic sites, the cathodic current is reduced, and thus total corrosion is reduced.[10] This behavior indicates that the semicircles correspond to an adsorption coating on the steel surface containing ZF-NPs. These deposits can result from a number of simple and complicated inorganic processes that produce chemicals that collect on metallic surfaces and are usually beneficial to improve inhibitory behavior.[52] Furthermore, the excellent corrosion resistance was attributed to the strong adhesion of paint films to the substrate, which was ascribed to strong homogeneity and high dispersion of nano pigments, which aids in their corrosion resistance. In addition, ferrite pigments can protect steel against corrosion by preventing corrosive elements from penetrating the layer. As a result, they can bind Cl^-, O_2, and H_2O, which are three of the most common causes of excessive corrosion.[53] Ferrites passivate steel substrates by creating an oxide layer with a stoichiometry like Fe_3O_4 on the surface. The hydrolysis of ferrite results in the creation of a passive layer on the steel that controls the medium. The corrosive processes on the cathode accelerate the hydrolysis of this pigment, which buffers the medium.

The Fe^{3+} oxide in the external layer can be hydrated, forming $Fe_2O_3 + H_2O$ or FeOOH, or oxyhydroxide FeOOH.[50] In this particular context, we want to make it clear that this behavior is deemed to be unique in comparison with the behavior of zinc ferrite that was manufactured in the bulk condition.[54]

Conclusions

Reddish inorganic nano pigment ''$ZnFe_2O_4$ NPs'' was successfully synthesized via facile sol–gel method. XRD measurements validated the produced pigment's single-phase spinel structure. The SEM/EDX results revealed that the crystalline particles are homogeneous, nano in size and extremely pure. The produced nanosized pigment has superior physicochemical properties than commercial bulk ones. The bandgap energy of ZF-NPs was measured to be 1.7 eV, and its reddish value (a^* = 41.8) was found to be comparable to that of M6001-iron oxide red used in commercial products. The printing ink containing inorganic nano pigments looked like commercial ink (M6001) with less pigmentation weight percent. Moreover, the coated film containing nano pigment has a promising corrosion resistance and high thermal stability. These results were reproducible and could be mass-produced at a reasonable cost on a massive scale. As a result, (ZF-NPs) has the potential to be an economically viable inorganic pigment with multiple applications in printing ink and paints industry.

Acknowledgments The authors would like to express the deepest appreciation to Dr. Walaa M. Abd El-Gawad, a researcher in Polymers and Pigments Department, National Research Centre, Cairo, Egypt for her valuable assistance in the implementation and interpretation of corrosion tests of this work.

Author contributions All authors contributed to the study conception and design. Material preparation, data collection and analysis were performed by [MAS] and [WMA]. The first draft of the manuscript was written by [MAS] and all authors commented on previous versions of the manuscript. All authors read and approved the final manuscript. Conceptualization, methodology, investigation, resources and writing—review and editing, were contributed by [MAS]. Conceptualization, Methodology, and investigation were contributed by [WMA]. Investigation, supervision were contributed by [SMT]. Investigation, resources were contributed by [AME]. Visualization, supervision were contributed by [MMA].

Funding Open access funding provided by The Science, Technology & Innovation Funding Authority (STDF) in cooperation with The Egyptian Knowledge Bank (EKB). No funds, grants, or other support was received.

Data availability Methods, including statements of data and materials availability and any associated accession codes and references, are available in the online version of this paper.

Conflict of interest All authors certify that they have no affiliations with or involvement in any organization or entity with any financial interest or non-financial interest in the subject matter or materials discussed in this manuscript.

References

1. Khanna, A, ''Functional Coatings by Incorporating Nanoparticles.'' *Nano Res*, **1** 1–8 (2015)
2. Vidales-Herrera, J, López, I, ''Nanomaterials in Coatings: An Industrial Point of View.'' In: *Handbook of Nanomaterials for Manufacturing Applications*, pp. 51–77. Elsevier (2020)
3. Chen, Y, Zhang, Y, Feng, S, ''Hydrothermal Synthesis and Properties of Pigments Chinese Purple $BaCuSi_2O_6$ and Dark Blue $BaCu_2Si_2O_7$.'' *Dyes Pigments*, **105** 167–173 (2014)
4. Mannari, V, Patel, C, *Paint Component. Understanding Raw Materials*. Vincentz Network, Hanover (2015)
5. Sørensen, PA, Kiil, S, Dam-Johansen, K, Weinell, CE, ''Anticorrosive Coatings: A Review.'' *J. Coat. Technol. Res.*, **6** 135–176 (2009)
6. Zhang, J, Cai, D, Qin, Y, Liu, D, Zhao, X, ''High Value-Added Monomer Chemicals and Functional Bio-Based Materials Derived from Polymeric Components of Lignocellulose by Organosolv Fractionation.'' *Biofuels Bioprod. Biorefin.*, **14** 371–401 (2020)
7. Lines, M, ''Nanomaterials for Practical Functional Uses.'' *J. Alloys Compd.*, **449** 242–245 (2008)
8. Thitsartarn, W, Jinkarn, T, ''Water Resistance Improvement of Paperboard by Coating Formulations Based on Nanoscale Pigments.'' *J. Coat. Technol. Res.*, **17** 1609–1617 (2020)
9. Candeia, R, Bernardi, M, Longo, E, Santos, I, Souza, A, ''Synthesis and Characterization of Spinel Pigment $CaFe_2O_4$

Obtained by the Polymeric Precursor Method.'' *Mater. Lett.*, **58** 569–572 (2004)
10. El-Ghaffar, A, Mahmoud, A, Ahmed, NM, Youssef, EA, ''A Method for Preparation and Application of Micronized Ferrite Pigments in Anticorrosive Solvent-Based Paints.'' *J. Coat. Technol. Res.*, **7** 703–713 (2010)
11. Abd El-Wahab, H, et al. ''Preparation and Evaluation of Nanosized Mixed Calcium Iron Oxide ($CaFe_2O_4$) as High Heat Resistant Pigment in Paints.'' *Pigment Resin Technol.*, **44** 172 (2015)
12. Brodinová, J, Stejskal, J, Kalendová, A, ''Investigation of Ferrites Properties with Polyaniline Layer in Anticorrosive Coatings.'' *J. Phys. Chem. Solids*, **68** 1091–1095 (2007)
13. Kalendová, A, Brodinova, J, ''Spinel and Rutile Pigments Containing Mg, Ca, Zn and Other Cations for Anticorrosive Coatings.'' *Anti-Corros. Methods Mater.*, **50** 352 (2003)
14. Zhao, Q, Yan, Z, Chen, C, Chen, J, ''Spinels: Controlled Preparation, Oxygen Reduction/Evolution Reaction Application, and Beyond.'' *Chem. Rev.*, **117** 10121–10211 (2017)
15. Bacorisen, D, et al. ''Atomistic Simulations of Radiation-Induced Defect Formation in Spinels: $MgAl_2O_4$, $MgGa_2O_4$, and $MgIn_2O_4$.'' *Phys. Rev. B*, **74** 214105 (2006)
16. Armelin, E, et al. ''Marine Paint Fomulations: Conducting Polymers as Anticorrosive Additives.'' *Prog. Org. Coat.*, **59** 46–52 (2007)
17. Béchade, E, et al. ''Synthesis of Lanthanum Silicate Oxyapatite Materials as a Solid Oxide Fuel Cell Electrolyte.'' *J. Eur. Ceram. Soc.*, **28** 2717–2724 (2008)
18. Bao, W, et al. ''Synthesis and Characterization of Fe^{3+} Doped $Co_{0.5}Mg_{0.5}Al_2O_4$ Inorganic Pigments with High Near-Infrared Reflectance.'' *Powder Technol.*, **292** 7–13 (2016)
19. Dippong, T, Levei, EA, Cadar, O, ''Recent Advances in Synthesis and Applications of MFe_2O_4 (M = Co, Cu, Mn, Ni, Zn) Nanoparticles.'' *Nanomaterials*, **11** 1560 (2021)
20. Sayed, MA, Abo-Aly, M, Aziz, AAA, Hassan, A, Salem, ANM, ''A Facile Hydrothermal Synthesis of Novel CeO_2/CdSe and CeO_2/CdTe Nanocomposites: Spectroscopic Investigations for Economically Feasible Photocatalytic Degradation of Congo Red Dye.'' *Inorg. Chem. Commun.*, **130** 108750 (2021)
21. Sayed, MA, Ahmed, M, El-Shahat, M, El-Sewify, IM, ''Mesoporous Polyaniline/SnO_2 Nanospheres for Enhanced Photocatalytic Degradation of Bio-staining Fluorescent Dye from an Aqueous Environment.'' *Inorg. Chem. Commun.*, **139** 109326 (2022)
22. Alifanti, M, et al. ''Characterization of CeO_2-ZrO_2 Mixed Oxides. Comparison of the Citrate and Sol−Gel Preparation Methods.'' *Chem. Mater.*, **15** 395–403 (2003)
23. Schwertmann, L, Wark, M, Marschall, R, ''Sol–Gel Synthesis of Defect-Pyrochlore Structured $CsTaWO_6$ and the Tribochemical Influences on Photocatalytic Activity.'' *RSC Adv.*, **3** 18908–18915 (2013)
24. Ngamcharussrivichai, C, Totarat, P, Bunyakiat, K, ''Ca and Zn Mixed Oxide as a Heterogeneous Base Catalyst for Transesterification of Palm Kernel Oil.'' *Appl. Catal. A Gen.*, **341** 77–85 (2008)
25. Hassan, A, et al. ''Synthesis, Characterization and Application of Mixed Metal Oxides Part $CaMnO_3$, $Ca_2Cr_2O_5$, $CaSb_2O_6$.'' *Egypt. J. Chem.*, **54** 447–461 (2011)
26. Fouad, OA, et al. ''Synthesis, Characterization and Application of Some Nanosized Mixed Metal Oxides as High Heat Resistant Pigments: Ca_2CuO_3, $Ca_3Co_2O_6$, and $NiSb_2O_6$.'' *J. Alloys Compd.*, **537** 165–170 (2012)
27. Pfaff, G, *Inorganic Pigments*. de Gruyter (2017)
28. Zhou, N, et al. ''Synthesis of High Near Infrared Reflection Wurtzite Structure Green Pigments Using Co-doped ZnO by Combustion Method.'' *Ceram. Int.*, **45** 3306–3312 (2019)
29. Abu Ayana, Y, El-Sawy, S, Salah, S, ''Zinc-Ferrite Pigment for Corrosion Protection.'' *Anti-Corros. Methods Mater.*, **44** 381–388 (1997)
30. Zhang, D, et al. ''A Facile Strategy for $ZnFe_2O_4$ Coating Preparing by Electrophoretic Deposition and Its Supercapacitor Performances.'' *J. Mater. Sci. Mater. Electron.*, **29** 5454–5458 (2018)
31. Kadhim, KJ, Lazem, TH, Blawa, BD, Mejbel, MK, ''Aluminium Substrates Coated by Mg-$ZnFe_2O_4$ Ferrite Using PVD Technique.'' *IOP Conf. Ser. Mater. Sci. Eng.*, **1105** 012042 (2021)
32. Ramadan, M, Amin, M, Sayed, MA, ''Superior Physico-Mechanical, Fire Resistivity, Morphological Characteristics and Gamma Radiation Shielding of Hardened OPC Pastes Incorporating $ZnFe_2O_4$ Spinel Nanoparticles.'' *Constr. Build. Mater.*, **234** 117807 (2020)
33. Abdelmaksoud, WM, Abualy, MM, Taleb, SM, ''Synthesis and Characterization of Novel Pigments Derived from Red Lake C.'' *Pigment Resin Technol.* (2019)
34. Abdelmaksoud, WM, Abualy, M, Teleb, S, Gabr, AM-E, Sayed, MA, ''Synthesis, Spectroscopic and Physico–Chemical Studies of Novel Pigments Derived from Lithol Rubine.'' *Pigment Resin Technol.*, **52** 593–600 (2022)
35. Egurrola, G, Segura, J, García, J, ''A New Analytical Method for the Evaluation of Cosmetic Pigments.'' *Color Res. Appl.*, **46** 821–829 (2021)
36. Illumination, I, ''Recommendations on Uniform Color Spaces.'' *Color-Difference Equations, Psychometric Color Terms, CIE* (1978)
37. Viezbicke, BD, Patel, S, Davis, BE, Birnie III, DP, ''Evaluation of the Tauc Method for Optical Absorption Edge Determination: ZnO Thin Films as a Model System.'' *Phys. Status Solidi (b)*, **252** 1700–1710 (2015)
38. Abdeldayem, HM, Sayed, MA, ''Synthesis and Characterization of Ag/Ce1-XBiXZnO Composites Hosted α-β/Bi_2O_3 as Highly Efficient Catalysts for Degradation of Cationic and Anionic Dyes.'' *J. Photochem. Photobiol. A Chem.*, **427** 113773 (2022)
39. Birgani, AN, Niyaifar, M, Hasanpour, A, ''Study of Cation Distribution of Spinel Zinc Nano-ferrite by X-ray.'' *J. Magn. Magn. Mater.*, **374** 179–181 (2015)
40. Patil, S, Bhojya Naik, H, Nagaraju, G, Viswanath, R, Rashmi, S, ''Synthesis of Visible Light Active Gd^{3+}-substituted $ZnFe_2O_4$ Nanoparticles for Photocatalytic and Antibacterial Activities.'' *Eur. Phys. J. Plus*, **132** 1–12 (2017)
41. Thandapani, P, Ramalinga Viswanathan, M, Denardin, JC, ''Magnetocaloric Effect and Universal Curve Behavior in Superparamagnetic Zinc Ferrite Nanoparticles Synthesized via Microwave Assisted Co-Precipitation Method.'' *Phys. Status Solidi (b)*, **215** 1700842 (2018)
42. Singh, A, et al. ''Synthesis, Characterization and Performance of Zinc Ferrite Nanorods for Room Temperature Sensing Applications.'' *J. Alloys Compd.*, **618** 475–483 (2015)
43. Dhiman, M, Sharma, R, Kumar, V, Singhal, S, ''Morphology Controlled Hydrothermal Synthesis and Photocatalytic Properties of $ZnFe_2O_4$ Nanostructures.'' *Ceram. Int.*, **42** 12594–12605 (2016)
44. Darwish, AS, Sayed, MA, Shebl, A, ''Cuttlefish Bone Stabilized Ag_3VO_4 Nanocomposite and Its Y_2O_3-Decorated Form: Waste-to-Value Development of Efficiently Eco-friendly Visible-Light-Photoactive and Biocidal Agents for Dyeing, Bacterial and Larvae Depollution of Egypt's

Wastewater.'' *J. Photochem. Photobiol. A Chem.*, **401** 112749 (2020)
45. Gramm, G, Fuhrmann, G, Wieser, M, Schottenberger, H, Huppertz, H, ''Environmentally Benign Inorganic Red Pigments Based on Tetragonal β-Bi_2O_3.'' *Dyes Pigments*, **160** 9–15 (2019)
46. Jose, S, Joshy, D, Narendranath, SB, Periyat, P, ''Recent Advances in Infrared Reflective Inorganic Pigments.'' *Solar Energy Mater. Solar Cells*, **194** 7–27 (2019)
47. Atta, AM, Shaker, N, Maysour, N, ''Influence of the Molecular Structure on the Chemical Resistivity and Thermal Stability of Cured Schiff Base Epoxy Resins.'' *Prog. Org. Coat.*, **56** 100–110 (2006)
48. Kotb, Y, et al. ''What Makes Epoxy-Phenolic Coatings on Metals Ubiquitous: Surface Energetics and Molecular Adhesion Characteristics.'' *J. Colloid Interface Sci.*, **608** 634–643 (2022)
49. Deshpande, PP, Jadhav, NG, Gelling, VJ, Sazou, D, ''Conducting Polymers for Corrosion Protection: A Review.'' *J. Coat. Technol. Res.*, **11** 473–494 (2014)
50. Ahmed, NM, Abd El-Gawad, WM, El-Shami, AA, Souaya, EM, ''Electrochemical Studies on the Corrosion Performance of New Advanced Anticorrosive Pigments.'' *Pigment Resin Technol.*, **46** 181–193 (2017)
51. Verma, A. et al. ''Mechanism, Anti-corrosion Protection and Components of Anti-Corrosion Polymer Coatings.'' In: *Polymer Coatings*, pp 53–66. CRC Press (2020)
52. Variola, F, et al. ''Improving Biocompatibility of Implantable Metals by Nanoscale Modification of Surfaces: An Overview of Strategies, Fabrication Methods, and Challenges.'' *Small*, **5** 996–1006 (2009)
53. Mohamed, MG, Ahmed, NM, Abd El-Gawad, WM, ''Corrosion Protection Performance of Reinforced Steel Coated with Paints Based on Waste Materials.'' *Anti-Corros. Methods Mater.*, **65** 368–374 (2018)
54. Ahmed, NM, Abd El-Gawad, WM, Souaya, ER, ''Study on the Corrosion Protection Performance of New Ferrite/Kaolin Core-Shell Pigments in Epoxy-Based Paints.'' *Anti-Corros. Methods Mater.,* **63** 36–46 (2015)